Available online at www.sciencedirect.com
ScienceDirect
Journal of Sound and Vibration 323 (2009) 93–111
JOURNAL OF SOUND AND VIBRATION
www.elsevier.com/locate/jsvi

Thermal post-buckled behaviors of cylindrical composite shells with viscoelastic damping treatments

Won-Ho Shin[a], Seung-Jun Lee[b], Il-Kwon Oh[c,*], In Lee[b,*,1]

[a]*Factory Automation, Manufacturing Technical Research Center, Samsung Electro-Mechanics, 314 Maetan-Dong, Yeongtong-Gu, Suwon, Gyunggi-Do 443-743, Republic of Korea*
[b]*Department of Aerospace Engineering, Korea Advanced Institute of Science and Technology, 373-1 Guseong-Dong, Yuseong-Gu, Daejeon 305-701, Republic of Korea*
[c]*School of Mechanical Systems Engineering, Chonnam National University, 300 Yongbong-dong, Buk-gu, Gwang-Ju 500-757, Republic of Korea*

Received 4 January 2008; received in revised form 12 August 2008; accepted 31 December 2008
Handling Editor: L.G. Tham
Available online 6 February 2009

Abstract

The finite element method for the vibration and damping analyses of the thermal post-buckled cylindrical composite shells with damping treatments was developed adopting the layerwise displacement field theory. The arc-length method was used to trace the nonlinear post-buckling behavior of the composite shell induced by the thermal load, and the complex modulus was adopted to consider the effects of the structural damping. The verification of the present results was performed in comparison with previous results, and the dynamic characteristics of several composite shells with damping treatments were investigated. The results show that the viscoelastic damping treatments could significantly affect the thermal post-buckling behaviors and the dynamic characteristics of the composite shells.

1. Introduction

It is well known that the dissipation of energy using viscoelastic damping materials within vibrating structures can reduce noise and vibration. Due to their importance in the design of the vibrating structures and systems, the vibrations of such damped systems have been investigated by many researchers [1–4]. Most early studies of damping treatments dealt with simple beams and plates. However, studies on the responses of cylindrical shells began to be undertaken as the demands of complex structures increased in various fields. Irie et al. [5] investigated the axisymmetrical response of a circular cylindrical double-shell system with internal damping by using a matrix analysis method based upon the Goldenveizer–Novozhilov theory. Lu et al. [6] performed experimental tests and a simple analysis of the forced vibratory response of a cylindrical shell with a

*Corresponding authors.
E-mail addresses: ikoh@chonnam.ac.kr (I.-K. Oh), inlee@asdl.kaist.ac.kr, inlee@kaist.ac.kr (I. Lee).
[1]Postal address: Division of Aerospace Engineering, Department of Engineering, Korea Advanced Institute of Science and Technology, 373-1 Guseong-Dong, Yuseong-Gu, Daejeon 305-701, Republic of Korea.

0022-460X/$ - see front matter © 2009 Elsevier Ltd. All rights reserved.
doi:10.1016/j.jsv.2008.12.029

Nomenclature

σ_{ij}	Cauchy stress tensor
f_i	body forces
ρ	density of structures
$\Phi^J(z)$	piecewise interpolation function through thickness direction
$\psi_I(\xi,\eta)$	finite element shape function
$\Psi_K^J(z)$	linear shape function
g	radius of cylindrical shell
u_i	displacements
U^J, V^J	in-plane displacement at the J-th interface
W	transverse displacement
Q_{ij}	elastic modulus
$\overline{Q}_{ij}$	reduced elastic modulus ($\overline{Q} = R^T Q R$)
$\mathbf{M}$	mass matrix
$\mathbf{K}^L$	linear stiffness matrix
$\mathbf{K}^{\Delta T}$	thermal geometric stiffness matrix
$\mathbf{K}^{N1}$	first order nonlinear stiffness matrix
$\mathbf{K}^{N2}$	second order nonlinear stiffness matrix
$\mathbf{F}^{\Delta T}$	thermal loading vector
$\mathbf{u}$	unknown displacement DOF vector
$\mathbf{q}$	out-of-balance vector
ΔT_{cr}	critical buckling temperature
ω_n	natural frequency of n-th mode
η_n	loss factor of n-th mode
$\mathbf{\Psi}_0$	normal mode vectors

number of axial beams adhered to it using a viscoelastic material layer. Their work showed good correlations between the test data and analytical solutions over a wide range of frequencies.

Sivadas and Ganesan [7,8] studied the effect of material damping on the dynamic stress response using the first order shell theory with shear deformation. Singh and Gupta [9,10] investigated the free vibration characteristics of a cylindrical tube by using the Timoshenko beam theory, thin shell theory, and first order deformation theory, and compared the results obtained from beam and shell theories. Ramesh and Ganesan [11–13] performed vibration and damping analyses of an orthotropic cylindrical shell with a constrained viscoelastic core using a finite element based on the discrete layer theory, and performed parametric studies of different core-to-facing thickness ratios, length-to-radius ratios, and boundary conditions. Okazaki et al. [14] studied the damping properties of cylindrical shells with an unconstrained viscoelastic layer, and Koo and Lee [15] developed the refined finite element model to describe the vibration and damping of anisotropic laminates in cylindrical bending. Xia and Lukasiewicz [16] investigated the effects of curvature radius, material properties, and layer thickness on the damping properties of sandwich cylindrical panels using the principle of virtual work.

Horacek and Kruntcheva [17] performed the finite element modeling of the damping characteristics of the cylindrical structure vibrating in a fluid and showed that the achieved agreement between the measured and calculated dynamic characteristics was good. Ramasamy and Ganesan [18] developed a finite element code based on the displacement field proposed by Wilkins [19] to observe the natural frequencies and loss factors of fluid-filled cylindrical shells with a constrained viscoelastic layer in between two facings made from composite material. Saravanan et al. [20] proposed a semianalytical finite element for doubly curved, multilayered shells of revolution based on an extension of Wilkins' displacement field. Ray et al. [21] investigated the effectiveness of active constrained layer damping treatments in enhancing the damping characteristics of thin cylindrical shells and performed experiments to verify their numerical predictions.

Chen and Huang [22] investigated the damping effects of a strip-type constrained layer damping treatment on a cylindrical shell using the assumed mode method. Lee et al. [23] investigated the dynamic characteristics of cylindrical composite panels with co-cured and constrained viscoelastic layers. Zheng et al. [24] optimized the layout of a passive constrained layer damping treatment to minimize the vibration response of cylindrical shells using the energy approach and assumed-mode method. They also studied the effects resulting from the number of patches, aspect ratios, and total amount of added passive constrained layer damping weight. Pradeep et al. [25] analyzed the buckling and vibration behavior of a viscoelastic sandwich cylinder in a thermal environment using the semi-analytical finite element method and the decoupled thermomechanical formulation.

The literature survey revealed that few papers were devoted to investigating the damping characteristics of cylindrical composite shells with damping layers, and to date the study on the thermal post-buckling of cylindrical composite panels with viscoelastic damping treatments has been not published. This paper

investigates the thermal post-buckled characteristics of cylindrical composite shells with viscoelastic layers. To fully consider the effects of viscoelastic damping and post-buckled behaviors subject to thermal loads, the transverse shear and variable in-plane displacements through the thickness are accurately modeled. In this study, the layerwise displacement theory and cylindrical arc-length method in the formulation of the finite element method, which has been verified previously in our research of composite plates [26,27,34] and cylindrical panels [23,28,31–33], are applied. This layerwise finite element model can provide accurate results for thermoelastic deformations and loss factors for various damping treatments of cylindrical composite shells with viscoelastic layers.

2. Layerwise finite element formulations

2.1. Description of layerwise displacement fields

Based on the layerwise laminate theory [23,28], the displacement fields (u, v, and w) on the $x-\phi-z$ coordinate system shown in Fig. 1 and temperature field can be expressed by introducing the following piecewise continuous approximations. By introducing the piecewise interpolation function along the thickness direction $\Phi^J(z)$ and the finite element shape function $\psi_I(\xi,\eta)$, the partial layerwise description of the displacements and the temperature distribution is given as follows:

$$u_1 = u(x,\phi,z,t) = \sum_{J=1}^{\mathrm{NID}} U^J(x,\phi,t)\Phi^J(z) = \sum_{J=1}^{\mathrm{NID}}\sum_{I=1}^{\mathrm{NPE}} U_I^J(x_I,\phi_I,t)\overline{\psi}_I(\xi,\eta)\Phi^J(z), \tag{1}$$

$$u_2 = v(x,\phi,z,t) = \sum_{J=1}^{\mathrm{NID}} V^J(x,\phi,t)\Phi^J(z) = \sum_{J=1}^{\mathrm{NID}}\sum_{I=1}^{\mathrm{NPE}} V_I^J(x_I,\phi_I,t)\overline{\psi}_I(\xi,\eta)\Phi^J(z), \tag{2}$$

$$u_3 = w(x,\phi,z,t) = \sum_{I=1}^{\mathrm{NPE}} W_I(x_I,\phi_I,t)\overline{\psi}_I(\xi,\eta), \tag{3}$$

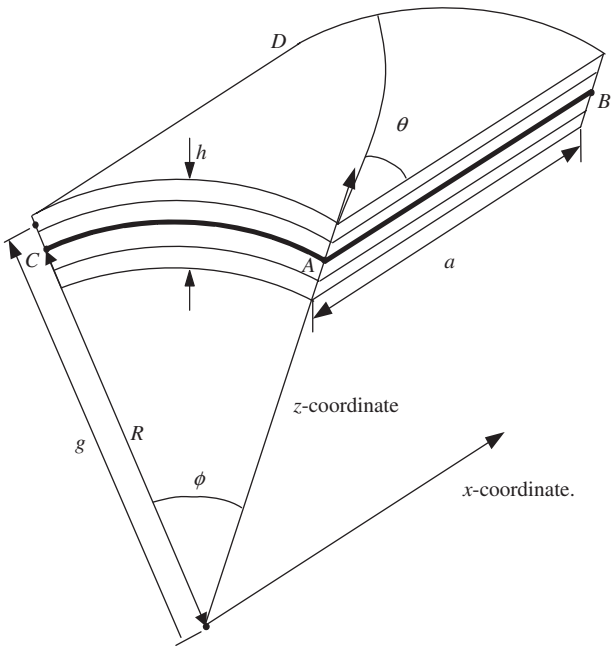

Fig. 1. Geometry of a cylindrical composite panel.

$$\Delta T(x,\phi,z,t)=\sum_{J=1}^{\mathrm{NID}}\sum_{I=1}^{\mathrm{NPE}}\Delta T_I^J(x_I,\phi_I,t)\overline{\psi}_I(\xi,\eta)\Phi^J(z) \tag{4}$$

where U^J, V^J and ΔT^J are the axial displacement, hoop displacement, and temperature increase at the J-th interface, respectively; W_I is the transverse displacement at the I-th node with the same value through the thickness direction. NID is the number of degrees of freedom for the in-plane displacement along the thickness direction for element i and NPE is the node number per element. The detailed interpolation function $\Phi^J(z)$ is defined with linear shape functions $\Psi_K^J(z)$ as follows:

$$\Phi^J(z)=\begin{cases}0 & \text{for } z<z_{J-1}\\ \Psi_2^{J-1}(z)=\dfrac{z-z_{J-1}}{z_J-z_{J-1}} & \text{for } z_{J-1}<z<z_J\\ \Psi_1^J(z)=-\dfrac{z-z_{J+1}}{z_{J+1}-z_J} & \text{for } z_J<z<z_{J+1}\\ 0 & \text{for } z_{J+1}<z\end{cases} \tag{5}$$

The sub-lamina concept of multi-layered structures with proper thickness discretization can be applied to reduce the computational time and memory storage required in the layerwise mechanics.

The *von Karman* nonlinear strain–displacement relationships were adopted to consider a large deflection due to thermomechanical loads. The relationships between strains and displacements can be written as follows:

$$\varepsilon_{xx}=\frac{\partial u}{\partial x}+\frac{1}{2}\left(\frac{\partial w}{\partial x}\right)^2=\sum_{J=1}^{N_i}\frac{\partial U^J}{\partial x}\Phi^J+\frac{1}{2}\left(\frac{\partial W}{\partial x}\right)^2, \tag{6}$$

$$\varepsilon_{\phi\phi}=\frac{\partial v}{g\partial\phi}+\frac{w}{g}+\frac{1}{2}\left(\frac{\partial w}{g\partial\phi}\right)^2=\sum_{J=1}^{N_i}\frac{\partial V^J}{g\partial\phi}\Phi^J+\frac{w}{g}+\frac{1}{2}\left(\frac{\partial W}{g\partial\phi}\right)^2, \tag{7}$$

$$\gamma_{x\phi}=\frac{\partial u}{g\partial\phi}+\frac{\partial v}{\partial x}+\frac{\partial w}{\partial x}\frac{\partial w}{g\partial\phi}=\sum_{J=1}^{N_i}\left(\frac{\partial U^J}{g\partial\phi}+\frac{\partial V^J}{g\partial\phi}\right)\Phi^J+\frac{\partial W}{\partial x}\frac{\partial W}{g\partial\phi}, \tag{8}$$

$$\gamma_{\phi z}=\frac{\partial w}{g\partial\phi}+\frac{\partial v}{\partial z}-\frac{v}{g}=\frac{\partial w}{g\partial\phi}+\sum_{J=1}^{N_i}V^J\frac{\mathrm{d}\Phi^J}{\mathrm{d}z}-\sum_{J=1}^{N_i}\left(\frac{V^J}{g}\right)\Phi^J, \tag{9}$$

$$\gamma_{xz}=\frac{\partial w}{\partial x}+\frac{\partial u}{\partial z}=\frac{\partial W}{\partial x}+\sum_{J=1}^{N_i}U^J\frac{\mathrm{d}\Phi^J}{\mathrm{d}z}. \tag{10}$$

where g means the radius of the cylindrical shell at an arbitrary interior position.

2.2. Constitutive equations of viscoelastic materials

The mechanical properties of the layered composite and viscoelastic materials are usually defined by a complex modulus; Young's modulus and the shear modulus can be expressed in the following forms:

$$\overline{E}_{ii}=E_{ii}(1+i\eta_{ii})\quad\text{for } i=1,2,3, \tag{11}$$

$$\overline{G}_{12}=G_{12}(1+i\eta_{12}),\quad \overline{G}_{23}=G_{23}(1+i\eta_{23}),\quad \overline{G}_{13}=G_{13}(1+i\eta_{13}). \tag{12}$$

In this study, all independent elastic and dissipative properties of the composite and viscoelastic plies are considered. Including the thermal effects, the unified linear constitutive equations for the k-th lamina between

the sinusoidal stresses and strains with respect to the material coordinate can be written as:

$$\begin{Bmatrix} \sigma_1 \\ \sigma_2 \\ \sigma_3 \\ \sigma_{23} \\ \sigma_{13} \\ \sigma_{12} \end{Bmatrix}_k = \begin{bmatrix} Q_{11} & Q_{12} & Q_{13} & 0 & 0 & 0 \\ Q_{12} & Q_{22} & Q_{23} & 0 & 0 & 0 \\ Q_{13} & Q_{23} & Q_{33} & 0 & 0 & 0 \\ 0 & 0 & 0 & Q_{44} & 0 & 0 \\ 0 & 0 & 0 & 0 & Q_{55} & 0 \\ 0 & 0 & 0 & 0 & 0 & Q_{66} \end{bmatrix}_k \left\{ \begin{Bmatrix} \varepsilon_1 \\ \varepsilon_2 \\ \varepsilon_3 \\ \varepsilon_{23} \\ \varepsilon_{13} \\ \varepsilon_{12} \end{Bmatrix} - \begin{Bmatrix} \alpha_1 \\ \alpha_2 \\ \alpha_3 \\ 0 \\ 0 \\ 0 \end{Bmatrix} \Delta T \right\}_k, \tag{13}$$

where

$$Q_{11} = (1 - v_{23}v_{32})/\overline{E}_{11}/\Delta, \quad Q_{12} = (v_{12} + v_{13}v_{32})\overline{E}_{22}/\Delta, \quad Q_{13} = (v_{13} + v_{12}v_{23})\overline{E}_{33}/\Delta,$$

$$Q_{23} = (v_{23} + v_{21}v_{13})\overline{E}_{33}/\Delta, \quad Q_{22} = (1 - v_{13}v_{31})\overline{E}_{22}/\Delta, \quad Q_{33} = (1 - v_{12}v_{21})\overline{E}_{33}/\Delta,$$

$$Q_{44} = \overline{G}_{23}, \quad Q_{55} = \overline{G}_{13}, \quad Q_{66} = \overline{G}_{12}, \quad \Delta = 1 - v_{12}v_{21} - v_{23}v_{32} - v_{13}v_{31} - 2v_{12}v_{23}v_{31}. \tag{14}$$

The corresponding constitutive relation for an anisotropic lamina referring to the initial configuration, $x - \phi - z$, can be obtained using the coordinate transformation with a fiber angle θ:

$$\begin{Bmatrix} \sigma_{xx} \\ \sigma_{\phi\phi} \\ \sigma_{zz} \\ \sigma_{\phi z} \\ \sigma_{xz} \\ \sigma_{x\phi} \end{Bmatrix}_k = \begin{bmatrix} \overline{Q}_{11} & \overline{Q}_{12} & \overline{Q}_{13} & 0 & 0 & \overline{Q}_{16} \\ \overline{Q}_{12} & \overline{Q}_{22} & \overline{Q}_{23} & 0 & 0 & \overline{Q}_{26} \\ \overline{Q}_{13} & \overline{Q}_{23} & \overline{Q}_{33} & 0 & 0 & \overline{Q}_{36} \\ 0 & 0 & 0 & \overline{Q}_{44} & \overline{Q}_{45} & 0 \\ 0 & 0 & 0 & \overline{Q}_{45} & \overline{Q}_{55} & 0 \\ \overline{Q}_{16} & \overline{Q}_{26} & \overline{Q}_{36} & 0 & 0 & \overline{Q}_{66} \end{bmatrix}_k \left\{ \begin{Bmatrix} \varepsilon_{xx} \\ \varepsilon_{\phi\phi} \\ \varepsilon_{zz} \\ \gamma_{\phi z} \\ \gamma_{xz} \\ \gamma_{x\phi} \end{Bmatrix} - \begin{Bmatrix} \overline{\alpha}_{xx} \\ \overline{\alpha}_{\phi\phi} \\ \overline{\alpha}_{zz} \\ 0 \\ 0 \\ \overline{\alpha}_{x\phi} \end{Bmatrix} \Delta T \right\}_k \tag{15}$$

where

$$\overline{Q}_{11} = Q_{11}m^4 + 2m^2n^2(Q_{12} + 2Q_{66}) + Q_{22}n^4, \quad \overline{Q}_{12} = m^2n^2(Q_{11} + Q_{22} - 4Q_{66}) + Q_{12}(m^4 + n^4),$$

$$\overline{Q}_{13} = Q_{13}m^2 + Q_{23}n^2, \quad \overline{Q}_{16} = -2Q_{66}mn(m^2 - n^2) + mn(Q_{12}m^2 + Q_{11}n^2) - mn(Q_{22}m^2 + Q_{12}n^2),$$

$$\overline{Q}_{22} = Q_{11}n^4 + 2m^2n^2(Q_{12} + 2Q_{66}) + Q_{22}m^4, \quad \overline{Q}_{23} = Q_{13}n^2 + Q_{23}m^2,$$

$$\overline{Q}_{26} = 2Q_{66}mn(m^2 - n^2) + mn(Q_{12}m^2 + Q_{11}n^2) - mn(Q_{22}m^2 + Q_{12}n^2), \quad \overline{Q}_{33} = Q_{33},$$

$$\overline{Q}_{36} = (Q_{13} - Q_{23})mn, \quad \overline{Q}_{44} = Q_{44}m^2 + Q_{55}n^2, \quad \overline{Q}_{45} = (Q_{55} - Q_{44})mn,$$

$$\overline{Q}_{55} = Q_{55}m^2 + Q_{44}n^2, \quad \overline{Q}_{66} = m^2n^2(Q_{11} - 2Q_{12} + Q_{22}) + Q_{66}(m^2 - n^2)^2, \tag{16}$$

where $m = \cos\theta$ and $n = \sin\theta$. The reduced constitutive equation can be written with the vector form from the assumption of zero transverse normal stress:

$$\boldsymbol{\sigma}_k = (\overline{\mathbf{Q}}_R + i\overline{\mathbf{Q}}_I)_k\boldsymbol{\varepsilon}_k - \overline{\boldsymbol{\alpha}}_k\Delta T, \tag{17}$$

where a subscript k indicates the layer number; $\overline{\mathbf{Q}}_R$ and $\overline{\mathbf{Q}}_I$ are the reduced real and imaginary stiffness matrices; $\overline{\boldsymbol{\alpha}}_k$ is the reduced coefficients of thermal expansion.

2.3. Derivation of governing equations

In order to derive the governing equation of motion for the cylindrical composite shells with viscoelastic layers, Hamilton's variational principle was applied in the following form:

$$\int_V (\rho \ddot{u}_i \delta u_i + \sigma_{ij} \delta \varepsilon_{ij} - f_i \delta u_i)\, \mathrm{d}V = \int_S \tau_i \delta u_i \, \mathrm{d}S, \tag{18}$$

where an infinitesimal volume of a cylinder is given as $\mathrm{d}V = g(z)\,\mathrm{d}\phi\,\mathrm{d}x\,\mathrm{d}z$. Over each finite element, the displacements were expressed as a linear combination of shape functions and nodal values on each finite element as the following form:

$$(W, U^J, V^J) = \sum_{k=1}^{\mathrm{NPE}} (W_k, U_k^J, V_k^J)\psi_k, \tag{19}$$

where NPE is the number of nodes per element. The shape functions, ψ_k, mean four, eight and nine nodes Lagrange elements. The nodal displacement vector for an element i can be defined as:

$$\mathbf{u}_e = \{\mathbf{u}^0 \;\; \mathbf{u}^1 \;\; \mathbf{v}^1 \;\; \mathbf{u}^2 \;\; \mathbf{v}^2 \;\; \cdots \;\; \mathbf{u}^{\mathrm{NID}} \;\; v^{\mathrm{NID}}\}^{\mathrm{T}}, \tag{20}$$

and

$$\mathbf{u}^0 = \{W_1 \;\; W_2 \;\; \cdots \;\; W_{\mathrm{NPE}}\}^{\mathrm{T}},$$

$$\mathbf{u}^J = \{U_1^J \;\; U_2^J \;\; \cdots \;\; U_{\mathrm{NPE}}^J\}^{\mathrm{T}}, \quad J = 1, 2, \ldots, N_i$$

$$\mathbf{v}^J = \{V_1^J \;\; V_2^J \;\; \cdots \;\; V_{\mathrm{NPE}}^J\}^{\mathrm{T}}. \tag{21}$$

Using variational formulations and finite elements, the nonlinear finite element equation of motion for the composite panels can be obtained by:

$$\mathbf{M}_e\ddot{\mathbf{u}}_e + (\mathbf{K}_{Re}^L - \mathbf{K}_{Re}^{\Delta T} + \tfrac{1}{2}\mathbf{K}_{Re}^{N1}(\mathbf{u}_e) + \tfrac{1}{3}\mathbf{K}_{Re}^{N2}(\mathbf{u}_e) + i(\mathbf{K}_{Ie}^L - \mathbf{K}_{Ie}^{\Delta T} + \tfrac{1}{2}\mathbf{K}_{Ie}^{N1}(\mathbf{u}_e) + \tfrac{1}{3}\mathbf{K}_{Ie}^{N2}(\mathbf{u}_e)))\mathbf{u}_e = \mathbf{F}_e^{\Delta T} + \mathbf{F}_e^{\mathrm{external}}, \tag{22}$$

where $\mathbf{M}_e$, $\mathbf{K}_e^L$, $\mathbf{K}_e^{\Delta T}$, $\mathbf{K}_e^{N1}$, $\mathbf{K}_e^{N2}$, $\mathbf{F}_e^{\Delta T}$, and $\mathbf{F}_e^{\mathrm{external}}$ are the mass matrix, linear stiffness, thermal geometric stiffness, first order nonlinear stiffness, second order nonlinear stiffness, thermal loading, and external force vectors, respectively. And the subscript R and I in the stiffness matrices mean real and imaginary in the complex values, respectively. The detailed real components of Eq. (22) have been given for mass, stiffness, and force vectors in our previous study [28]. Through the assembly procedure, the global finite element equation of laminated shells subject to the thermal load and the external load can be obtained as:

$$\mathbf{M}\ddot{\mathbf{u}} + (\mathbf{K}_R^L - \lambda_T\mathbf{K}_{R0}^{\Delta T} + \tfrac{1}{2}\mathbf{K}_R^{N1}(\mathbf{u}) + \tfrac{1}{3}\mathbf{K}_R^{N2}(\mathbf{u}) + i(\mathbf{K}_I^L - \lambda_T\mathbf{K}_{I0}^{\Delta T} + \tfrac{1}{2}\mathbf{K}_I^{N1}(\mathbf{u}) + \tfrac{1}{3}\mathbf{K}_I^{N2}(\mathbf{u})))\mathbf{u} = \lambda_T\mathbf{F}_0^{\Delta T} + \mathbf{F}^{\mathrm{external}}, \tag{23}$$

where $\mathbf{K}_0^{\Delta T}$, $\mathbf{F}_0^{\Delta T}$, and λ_T are the unit thermal geometric stiffness, force vector under a unit load level of temperature increase, and a load level, respectively. Also, $\mathbf{F}_0^{\mathrm{external}}$ is the force vector due to the external load. The thermal Euler buckling analysis was performed to determine the reference buckling temperature:

$$(\mathbf{K}_R^L - \Delta T_{\mathrm{cr}}\mathbf{K}_{R0}^{\Delta T})\boldsymbol{\Theta} = \mathbf{0}, \tag{24}$$

where ΔT_{cr} is the critical buckling temperature and $\boldsymbol{\Theta}$ is the buckling mode. The buckling mode shape is properly scaled as an initial estimated deflection to construct the nonlinear stiffness matrix in the post-buckled range. In order to analyze the thermoelastic post-buckling and small vibrations using the thermally buckled deflections, the solution of Eq. (23) is assumed to be the sum of the time-dependent and time-independent solutions such as $\mathbf{u} = \mathbf{u}_s + \mathbf{u}_t$, where $\mathbf{u}_s$ is the post-buckled large deflection and $\mathbf{u}_t$ is the time-dependent solution with a small amplitude. Substituting this assumed solution into Eq. (23), static and dynamic coupled

equations can be obtained as follows:

$$\mathbf{q}(\mathbf{u}_s, \lambda_T) = (\mathbf{K}_R^L + \tfrac{1}{2}\mathbf{K}_R^{N1}(\mathbf{u}) + \tfrac{1}{3}\mathbf{K}_R^{N2}(\mathbf{u}))\mathbf{u}_s - \lambda_T(\mathbf{K}_{R0}^{\Delta T}\mathbf{u}_s + \mathbf{F}_0^{\Delta T}) - \mathbf{F}_0^{\text{external}} = \mathbf{0} \tag{25}$$

$$\mathbf{M}\ddot{\mathbf{u}}_t + (\mathbf{K}_R^L - \lambda_T\mathbf{K}_{R0}^{\Delta T} + \tfrac{1}{2}\mathbf{K}_R^{N1}(\mathbf{u}_s) + \tfrac{1}{3}\mathbf{K}_R^{N2}(\mathbf{u}_s) + i(\mathbf{K}_I^L - \lambda_T\mathbf{K}_{I0}^{\Delta T} + \tfrac{1}{2}\mathbf{K}_I^{N1}(\mathbf{u}_s) + \tfrac{1}{3}\mathbf{K}_I^{N2}(\mathbf{u}_s)))\mathbf{u}_t = \mathbf{F}^{\text{external}}(t), \tag{26}$$

where $\mathbf{q}(\mathbf{u}_s, \lambda_T)$ is the out-of-balance vector. The static nonlinear governing Eq. (25) is solved by using the cylindrical arc-length method [28] to trace post-limit equilibrium curves of nonlinear responses of the cylindrical shells.

2.4. Free vibration including large deformation

The free vibration of the cylindrical composite panels with transverse large deflection can be obtained by solving the dynamic Eq. (26). However, the complex Eq. (26) has a lot of degree-of-freedoms and needs very long computational time. Therefore, the modal approach can be used to solve the complex eigen-value equation. The fundamental basis of the finite modal vectors can be found by solving the following equation:

$$(\mathbf{K}_R^L - \omega_n^2\mathbf{M})\mathbf{\Psi}_0 = 0 \tag{27}$$

Consequently, the reduced complex eigen-value equations of motion with generalized modal coordinate system can be obtained as follows (Fig. 2):

$$((\mathbf{K}^* + i\mathbf{K}_D^*) - \lambda_n^*\mathbf{M}^*)\mathbf{U}^* = \mathbf{0} \tag{28}$$

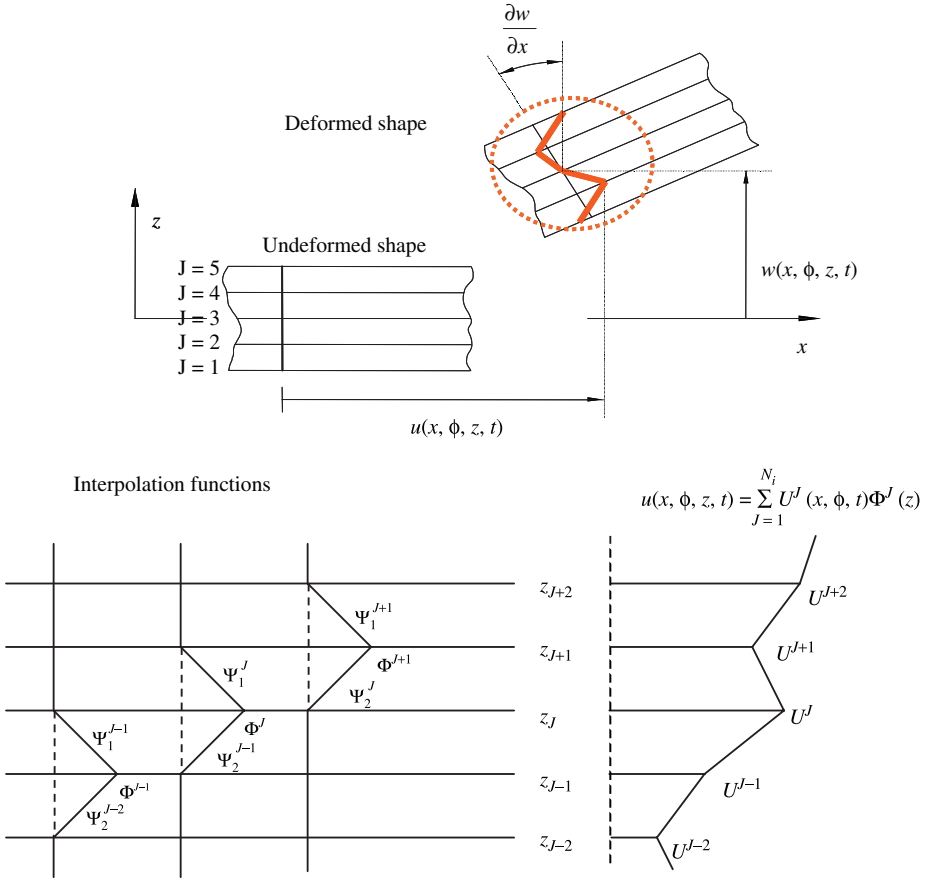

Fig. 2. Layerwise in-plane displacements and interpolation functions between layers of cylindrical shell.

where the reduced system matrices and vectors are given as:

$$\mathbf{M}^* = \boldsymbol{\Psi}_0^T \mathbf{M} \boldsymbol{\Psi}_0$$

$$\mathbf{K}^* = \boldsymbol{\Psi}_0^T (\mathbf{K}_R^L - \lambda_T \mathbf{K}_{R0}^{\Delta T} + \tfrac{1}{2}\mathbf{K}_R^{N1}(\mathbf{u}_s) + \tfrac{1}{3}\mathbf{K}_R^{N2}(\mathbf{u}_s)))\boldsymbol{\Psi}_0 \tag{29}$$

$$\mathbf{K}_D^* = \boldsymbol{\Psi}_0^T (\mathbf{K}_I^L - \lambda_T \mathbf{K}_{I0}^{\Delta T} + \tfrac{1}{2}\mathbf{K}_I^{N1}(\mathbf{u}_s) + \tfrac{1}{3}\mathbf{K}_I^{N2}(\mathbf{u}_s))\boldsymbol{\Psi}_0$$

$$\mathbf{U} = \boldsymbol{\Psi}_0 \mathbf{U}^*$$

From Eq. (28), the natural frequencies and loss factors for each mode are defined by real and imaginary parts of complex eigen-value λ_n^* in the following form

$$\omega_n^2 = \mathrm{Re}[\lambda_n^*], \quad \eta_n = \frac{\mathrm{Im}[\lambda_n^*]}{\mathrm{Re}[\lambda_n^*]}. \tag{30}$$

3. Results and discussion

3.1. Numerical validation of free vibration and thermal post-buckling analyses

3.1.1. Free vibration of a sandwich shell with a viscoelastic core

The numerical validation of a sandwich shell with a viscoelastic core was performed as shown in Fig. 3. The free vibration analyses based on the layerwise shell theory were performed and the results were compared with finite element solutions of Ramesh and Ganesan [11] using the discrete layer theory and high-order theory. Graphite/epoxy and PCV were chosen as the facing materials (subscript f) and the core (subscript c), respectively, and their properties are:

$$\text{Facings (graphite/epoxy)}: \; E_{1f} = 1.845 \times 10^{11}(1 + 0.000716i)\,\mathrm{N/m^2}, \quad \rho_f = 1600\,\mathrm{kg/m^3},$$

$$E_{2f} = 1.091 \times 10^{10}(1 + 0.00671i)\,\mathrm{N/m^2}, \quad E_{2f} = E_{3f}, \quad v_{12f} = v_{23f} = v_{13f} = 0.28,$$

$$G_{12f} = G_{23f} = G_{13f} = 7.31 \times 10^{9}(1 + 0.0112i)\,\mathrm{N/m^2}$$

$$\text{Core (PCV)}: \; E_c = 2.3 \times 10^{7}(1 + 0.3478i)\,\mathrm{N/m^2}, \quad v_c = 0.34, \quad \rho_c = 1350\,\mathrm{kg/m^3}$$

Generally, material properties are denoted as functions of environmental temperature and working frequency, however, for the convenience of validation in the present analyses, the properties are assumed

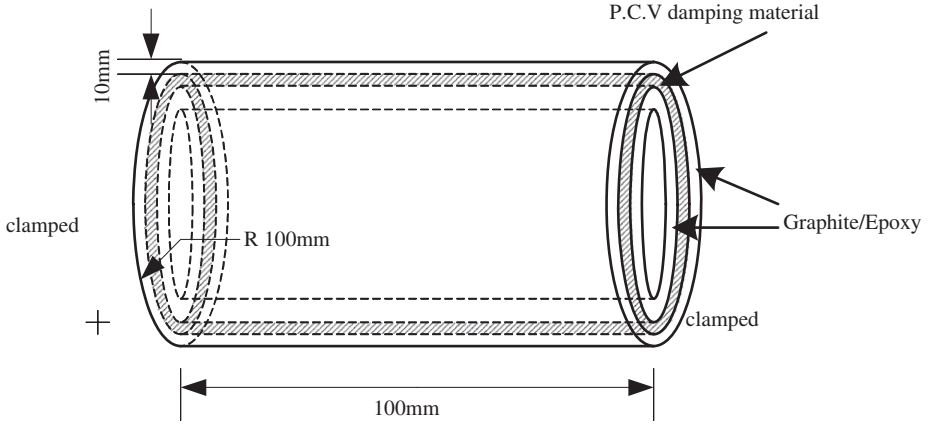

Fig. 3. Geometry information of cylindrical sandwich shell with viscoelastic core.

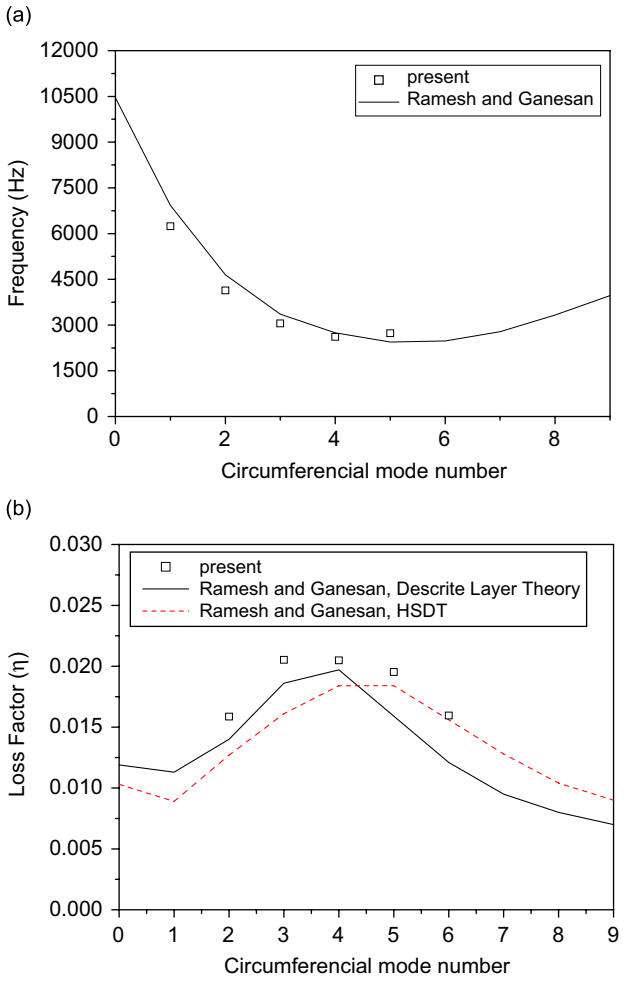

Fig. 4. Natural frequencies and loss factors of cylindrical sandwich shell with viscoelastic core: (a) natural frequency and (b) loss factor.

to be independent on the working frequency and environmental temperature and maintain constant values. The outer radius and length of the cylindrical shell, and the thickness of each layer are 100, 100, and 10 mm, respectively. The orientation angle of the fibers in the facings is 0° (longitudinal direction) and the boundary conditions are clamps at both ends. For the finite element analysis, the model used consists of 8×8 mesh with nine-node shell elements for the in-plane-direction and three sub-layers through the thickness.

In order to validate the code based on the layerwise field theory, the present results were compared with those obtained using the discrete layer theory and high-order theory. Fig. 4 indicates the natural frequencies and modal loss factors based on the layerwise shell theory and the results of Ramesh and Ganesan [11]; furthermore, these natural frequencies agree with the reference frequencies. The modal loss factors also follow the tendency of the reference loss factor although they were observed to be slightly higher than results of Ramesh and Ganesan's results [11].

3.1.2. Thermal post-buckling of the composite shell

The validation of the free vibration analysis results has already been proved in the previous section and the verification of the thermal post-buckling analysis results of the cylindrical composite shell are implemented in this section through a comparison with the results of Huang and Tauchert [30]. The geometry information and

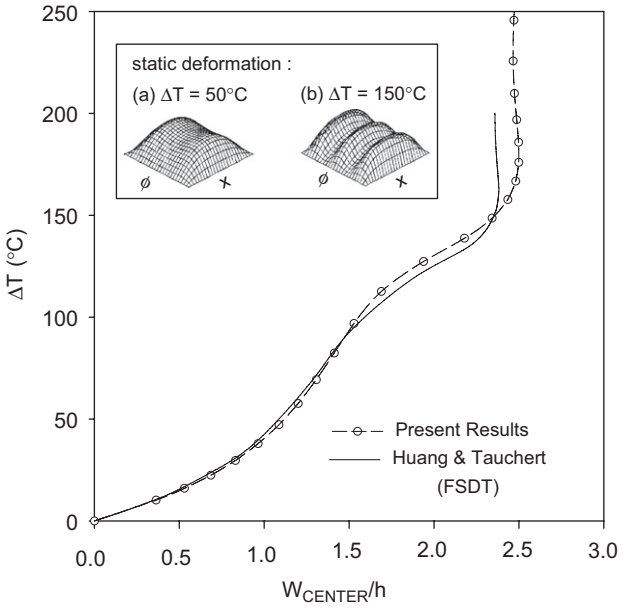

Fig. 5. Thermal post-bucking behaviors of cylindrical shell.

material properties of the cylindrical laminated shell are given as follows:

$$\text{Geometry information}: \quad \frac{a}{R\phi} = 1, \quad \frac{a}{h} = 200, \quad \frac{R}{a} = 5$$

$$\text{Material properties}: \quad E_1 = 138\,\text{Gpa}, \quad E_2 = E_3 = 8.28\,\text{Gpa}, \quad G_{12} = G_{13} = 6.9\,\text{Gpa}, \quad \nu_{23} = 0.373,$$
$$\nu_{12} = \nu_{13} = 0.33, \quad \rho = 1600\,\text{kg/m}^3, \quad \alpha_1 = 0.18 \times 10^{-6}/^{\circ}\text{C}, \quad \alpha_2 = \alpha_3 = 27 \times 10^{-6}/^{\circ}\text{C}.$$

The lamination consists of four zero-ply-angle layers with 0.125 mm thickness and all edges of shell are simply supported as follows:

$$W = V^J = U^m = 0 \quad \text{for } J = 1, N_i \text{ at } x = 0, a, \tag{31}$$

$$W = V^J = U^m = 0 \quad \text{for } J = 1, N_i \text{ at } R\phi = 0, a, \tag{32}$$

where m denotes the middle interface of the in-plane degree of freedom.

Fig. 5 indicates that the present results based on the layerwise theory resemble those of Huang and Tauchert [30], even though more flexible deflections in the highly nonlinear region were observed due to the in-plane flexibility in the present layerwise theory model. The W_{CENTER} in Fig. 5 means the transverse displacement of the cylindrical panel at the center point.

The validation problem considering both thermal post-buckling and structural damping was not found in the open literature. Therefore, in this study the verification of the present finite element code was independently performed by solving both the thermal post-buckling and structural damping of the cylindrical shells as compared in the Section 3.1.

3.2. Thermal post-buckling behaviors of a cylindrical shell with a viscoelastic layer

The thermal post-buckling behaviors of a cylindrical shell were investigated with various layer laminations, as shown in Fig. 6, which consist of laminate$_{1,2}$ and viscoelastic layers. Graphite/epoxy and 3M-ISD 112 were adopted for the face laminates (h_1,h_2) and viscoelastic layer (h_c), respectively. The properties of the

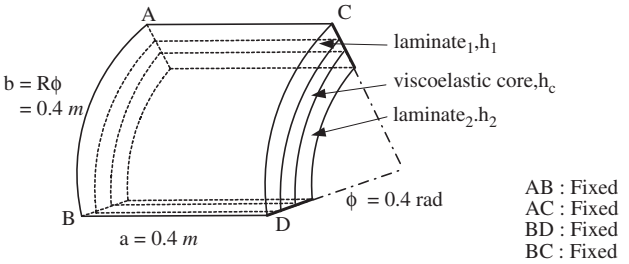

Fig. 6. Geometry and construction of cylindrical composite panels with viscoelastic layer.

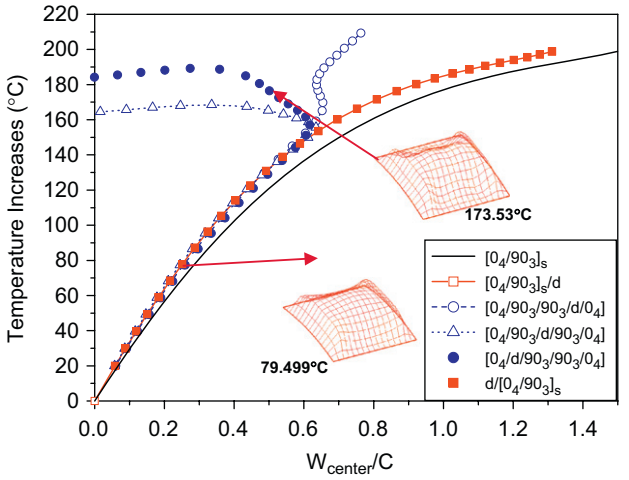

Fig. 7. Thermal post-bucking behaviors of cylindrical shell.

graphite/epoxy are:

$$E_1 = 119\,\text{Gpa}, \quad E_2 = 8.67\,\text{Gpa}, \quad G_{12} = G_{13} = 5.18\,\text{Gpa}, \quad G_{23} = 3.9\,\text{Gpa}, \quad v_{12} = 0.31,$$

$$\rho = 1570\,\text{kg/m}^3, \quad \eta_1 = 0.118\%, \quad \eta_2 = 0.620\%, \quad \eta_{12} = \eta_{13} = 0.812\%, \quad \eta_{23} = 0.846\%.$$

The properties of 3M-ISD 112 are denoted as a function of the environmental temperature and exciting frequency. The equations suggested by Drake [29] are given as:

$$\log_{10} M = \log_{10} M_L + \frac{2\log_{10} M_{\text{ROM}}/M_L}{1 + (FQ_{\text{ROM}}/FR)^{\text{SLOPE}}}, \tag{33}$$

$$\log_{10} \text{ETA} = \log_{10} \text{ETA}_{\text{FROL}} + \frac{C}{2}((S_H + S_L)A + (S_L - S_H)(1 - \sqrt{1 + A^2})), \tag{34}$$

where M (stiffness) and ETA (loss factor) can be calculated from Eqs. (33) and (34) to predict the material properties of 3M-ISD112. In this article, the environmental temperature and working frequency are assumed to be constant and degradation of the properties was not considered according to the various thermal loads.

The 12×12 meshes with nine node elements for the in-plane direction and five sub-laminates through the thickness direction were adopted for the finite element models. All edges (AB, CD, AC, and BD) of the cylindrical shell were clamped, and the clamps consisted of a 14-layered $[0_4/90_3]_s$ graphite/epoxy composite laminate of $400 \times 400 \times 1.75$ mm and a viscoelastic layer of $400 \times 400 \times 0.25$ mm. Fig. 7 elucidates the thermal post-buckling behaviors of several cylindrical shells as the sequences of the laminate with the damping layer are changed. The deformation of the central point of the $[0_4/90_3]_s$ laminate without a viscoelastic layer increased exponentially according to the increment of the thermal loads, and the shell structure had no

resistance for thermal loads over 200 °C. The results of the cases with the damping layer attached at the uppermost or lowermost graphite/epoxy layer have similar tendencies and show little improved thermal deformations due to the thickness increment compared with those of $[0_4/90_3]_s$. However, these cases also have weak thermal stability at temperature over 200 °C.

The changes of the thermally deformed shapes, which were not observed in the previous cases, occurred in the results of the laminates with an embedded damping layer when the thermal loading approached a specific temperature. The deformation of the central point of the $[0_4/90_3/90_3/d/0_4]$ laminate increased in the temperature regime below 170 and over 200 °C: in addition, the snap-through phenomenon was observed weakly between 170 and 200 °C. A region existed where the deformation of the central point decreased with respect to the temperature increments due to the metamorphosis of the thermally deformed shape. The structural endurance for the external thermal loading was improved substantially compared with the results of the composite shell without the damping layer.

The results of the $[0_4/d/90_3/90_3/0_4]$ laminate indicate different tendencies in the thermal deformation compared with those of $[0_4/90_3/90_3/d/0_4]$ in contrast to $[0_4/90_3]_s/d$ and $d/[0_4/90_3]_s$. The deformation of the central point of $[0_4/d/90_3/90_3/0_4]$ increased exponentially by 155 °C and then dropped shapely after the variation of the thermally deformed shape when the temperature rose. The static thermal trait was also enhanced compared with $[0_4/90_3]_s$. Finally, the deformation of the central point of the $[0_4/90_3/d/90_3/0_4]$ laminate, of which the damping layer was embedded into the central layer, is similar to the other results by

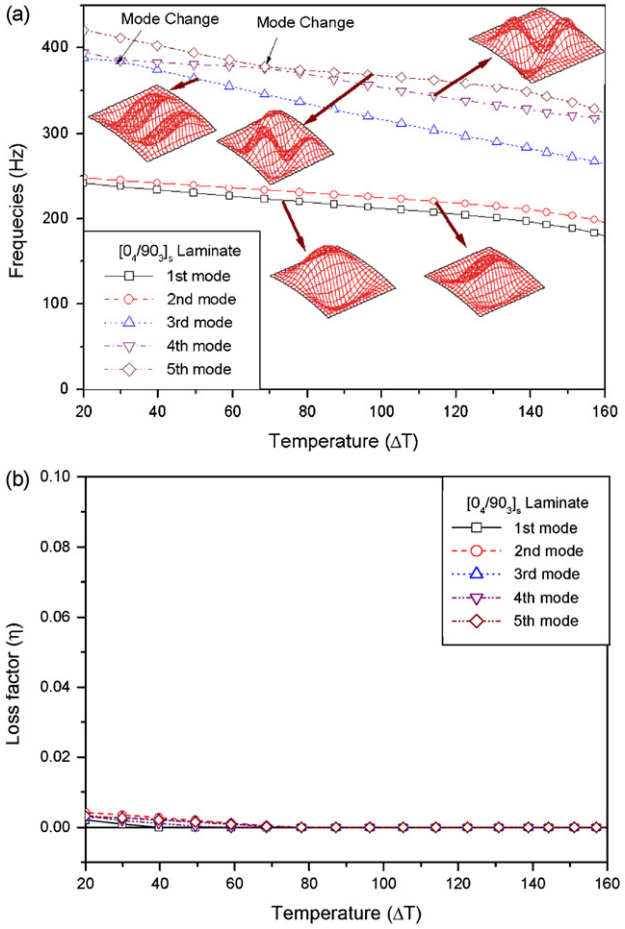

Fig. 8. Natural frequencies and loss factors of cylindrical shell $[0_4/90_3]_s$ according to thermal loading: (a) natural frequencies and (b) loss factors.

155 °C where the change of the thermally deformed shape occurred. The thermal deformation decreased more rapidly than those of $[0_4/d/90_3/90_3/0_4]$ with respect to temperature increments after the shape modification.

The present results show that the thermal deformation characteristics of several laminates with damping treatments improved compared with those of the laminates without a damping layer, and the sequences lamination of the viscoelastic layer may affect the thermal post-buckling behaviors. Unlike the base structural model and the free layer damping models, the constrained layer damping models show the unstable post-buckling behaviors.

3.3. Dynamic characteristics of cylindrical composite shell with a viscoelastic layer

Vibration analyses were implemented for the cylindrical composite shells with a viscoelastic layer, and the changes in the dynamic traits according to the various thermal loadings were investigated for the adopted schematic models in Section 3.2. The 12×12 meshes with nine node elements for the in-plane direction and five sub-laminates through the thickness were also used for the finite element models and all edges of cylindrical shell were clamped.

Fig. 8 presents the natural frequencies and modal loss factors of the $[0_4/90_3]_s$ laminate without a damping layer, d, when the thermal loading increased. The natural frequencies from the first to fifth modes declined

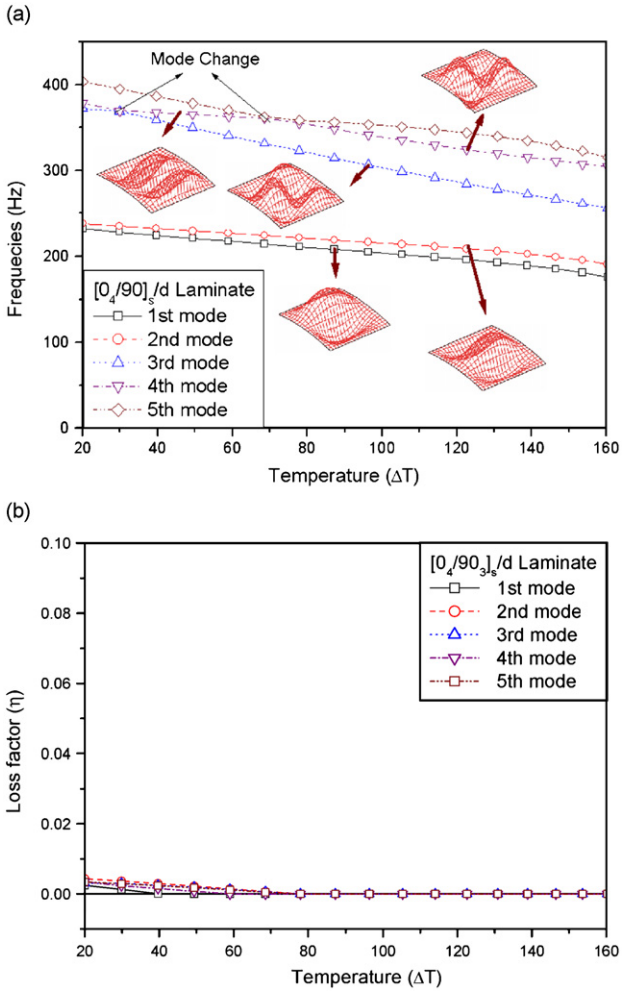

Fig. 9. Natural frequencies and loss factors of cylindrical shell $[0_4/90_3]_s/d$ according to thermal loading: (a) natural frequencies and (b) loss factors.

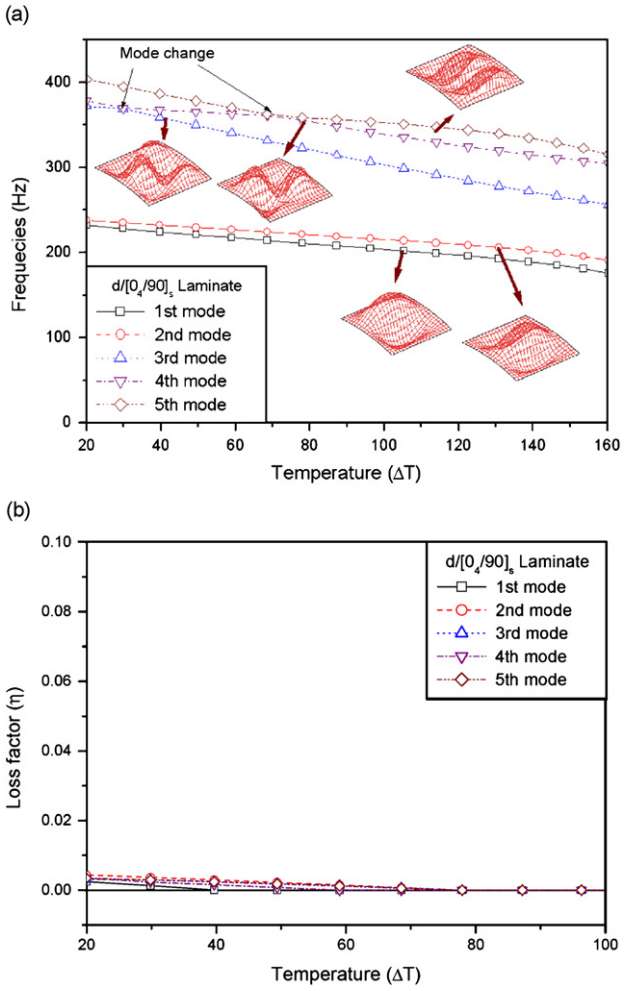

Fig. 10. Natural frequencies and loss factors of cylindrical shell $d/[0_4/90_3]_s$ according to thermal loading: (a) natural frequencies and (b) loss factors.

slightly when the temperature rose. M2N1, M3N1, M4N1, M3N2, and M2N2 are the mode shapes from the first to fifth modes without thermal loading. (M and N are defined as the number of circumferential modes and longitudinal modes, respectively.) The frequencies of the M3N2 and M2N2 modes decreased more rapidly than those of the other modes as the thermal loading increased due to the static deformations induced by thermal loading, as shown in Fig. 7, primarily occurring in the longitudinal direction and therefore weakening the longitudinal stiffness. The mode change between M4N1 and M3N2 occurs nearly near $\Delta T = 30\,^{\circ}\mathrm{C}$, and the curve veering phenomena between M4N1 and M2N2 occurs at approximately $\Delta T = 70\,^{\circ}\mathrm{C}$. In addition, the modal loss factors have a negligible value and converge to zero with the thermal loading increments. Figs. 9 and 10 show the natural frequencies and modal loss factors of the cylindrical composite shells with damping layers attached to the uppermost layer or the lowermost layer. For the $[0_4/90_3]_s/d$ laminate, the natural frequencies were reduced slightly in comparison with those of the $[0_4/90_3]_s$ laminate due to the mass of the damping layer, and the mode changes among M4N1, M3N2, and M2N2 were also observed at approximately $\Delta T = 30, 70\,^{\circ}\mathrm{C}$. The increments of the modal loss factors induced by the damping layer were negligible, and the magnitudes of the loss factors converged to zero with the temperature rise. The dynamic characteristics of the $d/[0_4/90_3]_s$ laminate showed similar tendencies to those of the $[0_4/90_3]_s/d$ laminate.

Fig. 11 presents the natural frequencies and the modal loss factors of the $[0_4/90_3/90_3/d/0_4]$ laminate: the declines of the natural frequencies are shown compared with those of the previous cases. M3N2 and M2N2

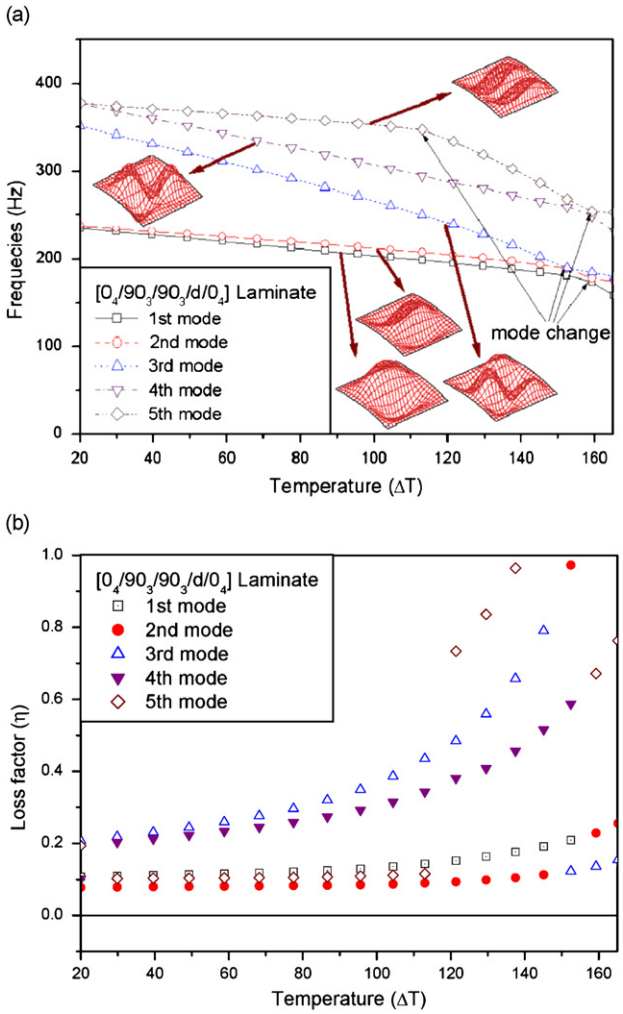

Fig. 11. Natural frequencies and loss factors of cylindrical shell $[0_4/90_3/90_3/d/0_4]$ according to thermal loading: (a) natural frequencies and (b) loss factors.

which were the fourth and fifth modes in the previous cases are observed as the third and fourth modes, and M4N1 is now the fifth mode. All natural frequencies decreased smoothly; furthermore, M3N2 and M2N2 diminished faster than the other modes with the increments of thermal loading. The mode change between M4N1 and the higher modes was observed around $\Delta T = 110\,^{\circ}\mathrm{C}$, and the complicated natural frequency curves were entangled near $\Delta T = 150-160\,^{\circ}\mathrm{C}$. This may be due to the static deformation shape changing as the thermal loading changed above $\Delta T = 150\,^{\circ}\mathrm{C}$, and the variation of the structural shape affects the dynamic characteristics of the laminate shell as shown in Fig. 7. The modal loss factors induced by the damping layer were remarkably improved, and the magnitudes of the loss factors increased with the temperature rise in contrast to Figs. 8(b)–10(b).

The modal loss factors of M3N2 and M2N2 were larger than M2N1, M3N1 and M3N2, and the former increased more rapidly than the latter according to the thermal loading. These results indicate that the thermal loads affect the longitudinal dynamic characteristics more preferentially.

The dynamic traits of the $[0_4/d/90_3/90_3/0_4]$ laminate, as shown in Fig. 12, are adapted to the tendencies of the $[0_4/90_3/90_3/d/0_4]$ laminate below the temperature where the shape change of the thermal static deformation occurs, except the mode change temperature. However, in the realm above $\Delta T = 150\,^{\circ}\mathrm{C}$, Fig. 12(a) shows that the curves of the natural frequencies are more intricate than those of Fig. 11(a). This may be due to the

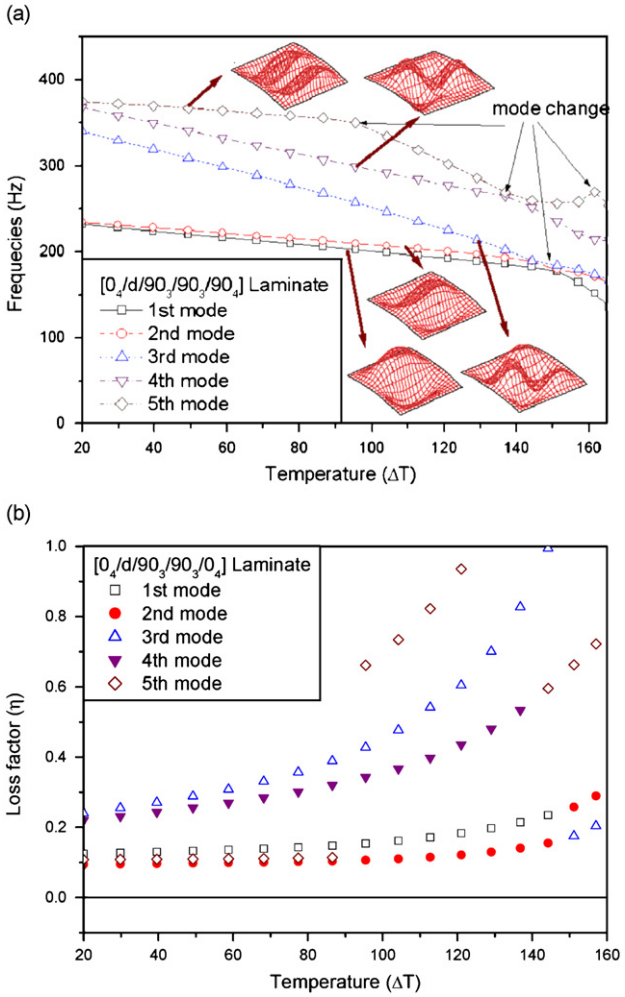

Fig. 12. Natural frequencies and loss factors of cylindrical shell $[0_4/d/90_3/90_3/0_4]$ according to thermal loading: (a) natural frequencies and (b) loss factors.

thermal deformation of the $[0_4/90_3/90_3/d/0_4]$ laminate changing to another type from $\Delta T = 150$ to $180\,^{\circ}C$, and then it returns to its original shape above $\Delta T = 180\,^{\circ}C$, whereas those of the $[0_4/d/90_3/90_3/0_4]$ laminate change to a completely different shape above $\Delta T = 150\,^{\circ}C$. The modal loss factors of the $[0_4/d/90_3/90_3/0_4]$ improve slightly in comparison with those of the $[0_4/90_3/90_3/d/0_4]$. These results show that the effect of the thermally deformed shape on the dynamic characteristics is significant.

Fig. 13 indicates the natural frequencies and modal loss factors of the $[0_4/90_3/d/90_3/0_4]$ laminate, and the natural frequencies have lower values than any other laminate previously mentioned here. M3N2, M4N1, and M2N2 are observed as the third, fourth, and fifth modes, respectively. All natural frequencies decreased smoothly; in addition, M3N2 and M2N2 diminished faster than the other modes with the increments of thermal loading below $\Delta T = 150\,^{\circ}C$. The mode change between M4N1 and the higher modes was observed near $\Delta T = 120\,^{\circ}C$, and the mode conversion between M3N1 and M3N2 modes was also observed at a similar temperature.

The natural frequency curves showed similar tendencies to the graphs in Figs. 11(a) and 12(a) below $\Delta T = 150\,^{\circ}C$. However, all natural frequencies dropped sharply above $\Delta T = 150\,^{\circ}C$, and more complicated natural frequency curves entangled one another at $\Delta T = 150-160\,^{\circ}C$. This may be why the thermally deformed shape was converted to another shape at $\Delta T = 150-160\,^{\circ}C$, and the conversion of the thermally deformed shape influences the structural stiffness of the laminate shell. The modal loss factors induced by the

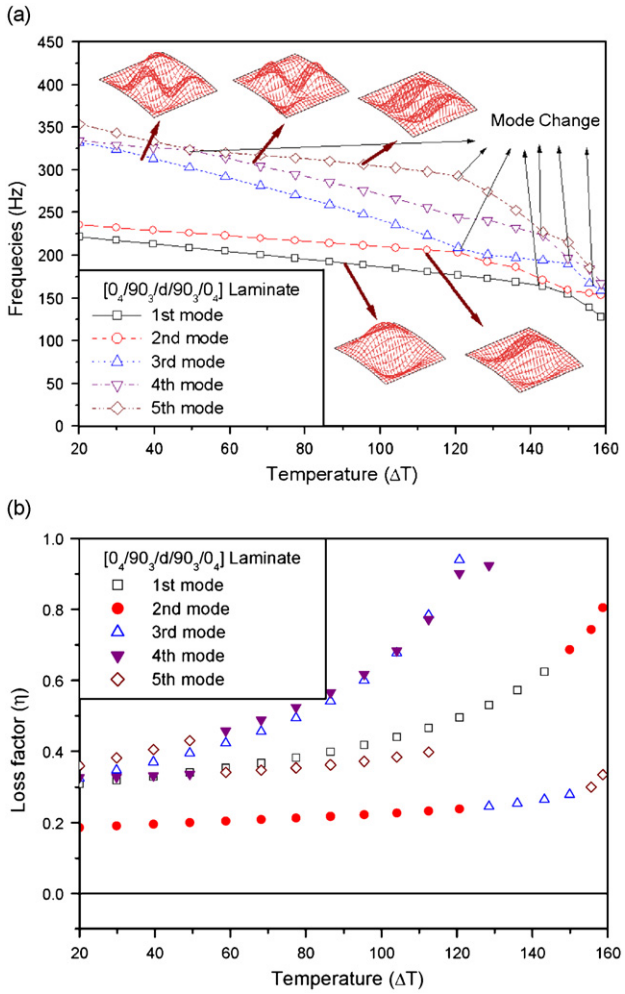

Fig. 13. Natural frequencies and loss factors of cylindrical shell $[0_4/90_3/d/90_3/0_4]$ according to thermal loading: (a) natural frequencies and (b) loss factors.

damping layer were the most improved among all laminates, and the magnitudes of the loss factors considerably increased with temperature rises except M21. The modal loss factor of M21 increased smoothly according to the thermal loading. The results show that the thermal loads can affect the dynamic characteristics of the higher modes more significantly than those of the first mode. The constrained layer damping models show much higher damping loss factors than that of the free layer damping models. Also, as the temperature increases, the damping loss factor shows an increasing trend in the constrained and sandwiched models. It means that the thermal stresses and deformations increase the shear deformation of the constrained and sandwiched models, resulting in the increasing trend of the damping loss factor.

4. Conclusion

In present study, the dynamic characteristics of a cylindrical composite shell were investigated using a layerwise finite element method when the structural damping treatments and thermal post-buckled behaviors were coupled. The analysis code was developed adopting the layerwise displacement field theory, complex modulus, and arc-length method; furthermore, the results were verified when compared with previous results. The natural frequencies and modal loss factors of the composite shells were investigated according to the laminating sequences as the thermal loading increased. The present results indicate that the damping

treatments can significantly affect thermal post-buckling behaviors, and the thermally deformed shapes may strongly influence the dynamic characteristics of the composite shells. In addition, the results show that the modal loss factors can be improved through damping treatments but the natural frequencies and thermal post-buckling characteristics may become worsen.

Acknowledgments

This work was partially supported by the second stage of the Brain Korea 21 Project in 2007. Also, this work was partially supported by the Korea Science and Engineering Foundation (KOSEF) NRL Program grant funded by the Korea government (MEST) (no. R0A-2008-000-20012-0).

References

[1] E.M. Kerwin Jr., Damping of flexural waves by a constrained viscoelastic layer, *Journal of the Acoustical Society of America* 31 (1959) 952–962.
[2] R.A. Ditaranto, Theory of vibratory bending for elastic and viscoelastic layered finite-length beams, *Journal of Applied Mechanics* 32 (1965) 881–886.
[3] D.J. Mead, S. Markus, The forced vibration of a three-layer damped sandwich beam with arbitrary boundary conditions, *Journal of Sound and Vibration* 10 (1969) 163–175.
[4] J.E. Ruzwka, Damping structural resonances using viscoelastic shear-damping mechanisms, part 1—design configurations, *Journal of Engineering for Industry* 83 (1961) 403–413.
[5] T. Ire, G. Yamada, Y. Muramoto, The axisymmetrical response of a circular cylindrical double-shell system with internal damping, *Journal of Sound and Vibration* 92 (1) (1984) 107–115.
[6] Y.P. Lu, A.J. Roscoe III, B.E. Douglas, Analysis of the response of damped cylindrical shells carrying discontinuously constrained beam elements, *Journal of Sound and Vibration* 150 (3) (1991) 395–403.
[7] K.R. Sivadas, N. Ganesan, Dynamic analysis of circular cylindrical shells with material damping, *Journal of Sound and Vibration* 166 (1) (1993) 395–403.
[8] K.R. Sivadas, N. Ganesan, Free vibration and material damping analysis of moderately thick circular shells, *Journal of Sound and Vibration* 172 (1) (1994) 47–61.
[9] S.P. Singh, K. Gupta, Free damped flexural vibration analysis of composite cylindrical tubes using beam and shell theory, *Journal of Sound and Vibration* 172 (2) (1994) 171–190.
[10] S.P. Singh, K. Gupta, Damped free vibration layered composite cylindrical shells, *Journal of Sound and Vibration* 172 (2) (1994) 191–209.
[11] T.C. Ramesh, N. Ganesan, Orthotropic cylindrical shells with a viscoelastic core: a vibration and damping analysis, *Journal of Sound and Vibration* 175 (4) (1994) 535–555.
[12] T.C. Ramesh, N. Ganesan, The harmonic response of cylindrical shells with constrained damping treatment, *Journal of Sound and Vibration* 180 (5) (1995) 745–756.
[13] T.C. Ramesh, N. Ganesan, Influence of constrained damping layer on the resonant response of orthotropic cylindrical shells, *Journal of Sound and Vibration* 185 (3) (1995) 483–500.
[14] A. Okazaki, A. Tatemichi, S. Mirza, Damping properties of two-layered cylindrical shells with an unconstrained viscoelastic damping, *Journal of Sound and Vibration* 176 (2) (1994) 145–161.
[15] K.N. Koo, I. Lee, A refined analysis of vibration and damping for anisotropic laminates in cylindrical bending, *Journal of Sound and Vibration* 184 (4) (1995) 553–566.
[16] Z.Q. Xia, S. Lukasiewicz, Non-linear analysis of damping properties of cylindrical sandwich panels, *Journal of Sound and Vibration* 186 (1) (1995) 55–69.
[17] J. Horacek, M. Kruntcheva, Finite element modeling of the damping of cylindrical shells vibrating in contact with an annular fluid region, *Journal of Sound and Vibration* 203 (4) (1997) 723–727.
[18] R. Ramasamy, N. Ganesan, Vibration and damping analysis of fluid filled orthotropic cylindrical shells with constrained viscoelastic damping, *Computers and Structures* 70 (3) (1999) 363–376.
[19] D.J. Wilkins Jr., C.W. Bert, D.M. Egle, Free vibrations of orthotropic sandwich conical shells with various boundary conditions, *Journal of Sound and Vibration* 13 (1970) 211–228.
[20] C. Saravanan, N. Ganesan, V. Ramamurti, Vibration and damping analysis of multilayered fluid filled cylindrical shells with constrained viscoelastic damping using modal strain energy method, *Computers and Structures* 75 (4) (2000) 395–417.
[21] M.C. Ray, J. Oh, A. Baz, Active constrained layer damping of thin cylindrical shells, *Journal of Sound and Vibration* 240 (5) (2001) 921–935.
[22] L.H. Chen, S.C. Huang, Vibration attenuation of a cylindrical shell with constrained layer damping strips treatment, *Computers and Structures* 79 (14) (2001) 1355–1362.
[23] I. Lee, I.K. Oh, W.H. Shin, K.D. Cho, K.N. Koo, Dynamic characteristics of cylindrical composite panels with co-cured and constrained viscoelastic layers, *JSME International Journal Series C* 45 (2002) 16–25.

[24] H. Zheng, C. Cai, G.S.H. Pau, G.R. Liu, Minimizing vibration response of cylindrical shells through layout optimization of passive constrained layer damping treatments, *Journal of Sound and Vibration* 279 (3) (2005) 739–756.
[25] V. Pradeep, N. Ganesan, C. Padmanabhan, Buckling and vibration behavior of a viscoelastic sandwich cylinder under thermal environment, *International Journal for Computational Methods in Engineering Science and Mechanics* 7 (2006) 389–401.
[26] I.K. Oh, J.H. Han, I. Lee, Postbuckling and vibration characteristics of piezolaminated composite plate subject to thermo-piezoelectric loads, *Journal of Sound and Vibration* 233 (2000) 19–40.
[27] I.K. Oh, J.H. Han, I. Lee, Thermopiezoelastic snapping of piezolaminated plates using layerwise nonlinear finite elements, *AIAA Journal* 39 (2001) 1188–1198.
[28] I.K. Oh, I. Lee, Thermal snapping and vibration characteristics of cylindrical composite panels using layerwise theory, *Composite Structures* 51 (2001) 49–61.
[29] M.L. Drake, Damping properties of various materials, Technical Report AFWAL-TR-88-4248, 1989.
[30] N.N. Huang, T.R. Tauchert, Large deflections of laminated cylindrical and doubly curved panels under thermal loading, *Computers & Structures* 41 (1991) 303–312.
[31] I.K. Oh, Dynamic characteristics of cylindrical hybrid panels containing viscoelastic layer based on layerwise mechanics, *Composites Part B: Engineering* 38 (2) (2007) 159–171.
[32] I.K. Oh, Piezoelectric suppression of thermoelastic snap-through of active piezolaminated curved shells, *Smart Materials and Structures* 15 (6) (2006) 1616–1626.
[33] I.K. Oh, I. Lee, Supersonic flutter suppression of cylindrical piezolaminated panels using multi-field layerwise theory, *Journal of Sound and Vibration* 291 (3–5) (2006) 1186–1201.
[34] I.K. Oh, Thermopiezoelastic nonlinear dynamics of active piezolaminated plates, *Smart Materials and Structures* 14 (2005) 823–834.